Truncation Robust C-Arm CT Reconstruction for Dynamic Collimation Acquisition Schemes

Thomas Kästner[1], Joachim Hornegger[1], Andreas Maier[1], Yan Xia[1], Sebastian Bauer[2]

[1]Friedrich-Alexander Universität Erlangen-Nürnberg
[2]Siemens AG, Forchheim, Germany
thom.kaestner@gmail.com

Abstract. Volume-of-interest (VOI) C-arm computed tomography (CT) imaging is a promising approach to acquire anatomical information in a pre-defined target volume at low dose, using both axial and trans-axial collimation. However, also the region outside the target volume, below referred to as peripheral region (PR), could contain some valuable information for image guidance. The potential use of a fast dynamically changing collimator would allow for new acquisition schemes, that acquire projection data in a way that allows for both a high-quality reconstruction of the diagnostic VOI and a low-quality reconstruction of the peripheral region, still at a low overall dose. In this paper, we present a novel reconstruction algorithm for an acquisition scheme that acquires a large portion of the projections in a collimated manner, while acquiring a small portion of the projections in a non-collimated manner. Experimental results indicate that few non-truncated projections can help to improve the image quality compared to a conventional VOI acquisition, while simultaneously providing valuable information about the peripheral region.

1 Introduction

Reducing dose while maintaining image quality has become an emerging field in CT imaging and a general rule for any practical medical X-ray imaging application. In some clinical applications, in particular in image guided therapy, only a small portion of the patient is required to be examined. A promising approach is Volume of Interest (VOI) computed tomography (CT). In order to reduce the field of view (FOV) to the region-of-interest (ROI), an X-ray beam collimator is deployed to laterally and axially block the radiation during the scan. As a consequence, VOI imaging results in truncated projections which pose a challenge to conventional 3D cone beam reconstruction algorithms. Furthermore, no information of the region outside the VOI, the peripheral region (PR), is provided. However, some knowledge about the PR could be helpful in image-guided therapy and interventional procedures. Certain procedures require a high image quality of the VOI, while a low image quality of the PR might be sufficient. Even though that would involve the acquisition of a sparse set of

H. Handels et al. (Hrsg.), *Bildverarbeitung für die Medizin 2015,* Informatik aktuell,
DOI 10.1007/978-3-662-46224-9_88,

non-truncated projections, the overall applied dose would remain well below the amount of a conventional scan. When it comes to the deployment of an implant for instance, not only the VOI but also the PR may contain relevant information. This information might be helpful in image guided procedures in order to reach the target location. Another application could be in cancer or tumor treatment, where the PR covers organs-at-risk, holding valuable information to optimize the treatment plan.

Leary and Robar [1] demonstrated the acquisition of multiple volumes, an inner VOI and a nested VOI. In particular, they performed one acquisition and modified the collimation during the scan. The projection data was processed using the conventional FDK [2] algorithm in combination with an extrapolation [3] of the truncated projection data, followed by an additional normalization of relative image intensity of the inner and the nested VOI. However, as stated in the paper, the approach does not preserve HU values compared to the FDK reconstruction of non-truncated data.

In this paper, we performed a simulation study of a new acquisition scheme that provides truncated and non-truncated projections within one scan. To our knowledge, no reconstruction algorithms have been developed so far that are specifically dedicated to this kind of acquisition scheme. This work introduces a novel algorithm that is capable to reconstruct such data, yielding both a high-quality VOI reconstruction and a low-quality PR reconstruction.

2 Materials and methods

2.1 Acquisition scheme

In this work, which is a simulation study, we made use of the concept of a dedicated acquisition scheme (Fig. 1). It acquires two sets of different projections, non-truncated and truncated projections. In practice, this would require a fast dynamic collimator that blocks the radiation both axially and laterally during a C-arm CT acquisition and that is capable of changing its size dynamically over the entire possible range, while the C-arm is rotating from one angular position to another. While the FOV is collimated to the ROI for most projection angles, every n-th frame the collimator opens completely to acquire a non-truncated projection. This results in a sparse number of full FOV projections and a dense number of ROI projections, within one single scan. In this context, let us introduce the term sparsity, referring to the frequency of full projections. For instance,

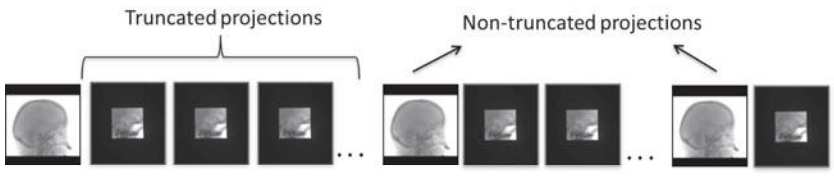

Fig. 1. Schematic illustration of the acquisition scheme.

a sparsity of $k = 10$ corresponds to an acquisition protocol where every 10-th projection is a full projection. The parameter k is calculated by dividing the total number of acquired projections by the number of acquired full projections.

2.2 FDK reconstruction

From our simulated acquisition scheme we obtain two data sets, a dense set of truncated projections and a sparse set of non-truncated projections. In a first step, we perform an initial reconstruction of the sparse set of non-truncated projections. To this end, we use an iterative total-variation (iTV) based algorithm [4] to obtain acceptable reconstruction results from such sparse data. In a second step, we perform a forward projection of the initial reconstruction to de-truncate the subset of truncated projections. The forward projections are being adapted by using the unprocessed truncated projection data. That way, we obtain a full set of non-truncated data, consisting of a dense set of detruncated projection data as well as the sparse set of non-truncated projection data, being eventually backprojected along the lines of a conventional FDK algorithm [2]. An illustrative overview of the algorithm is given in Fig. 2. Below, we elaborate on the individual processing steps.

Adaption and transition weighting We perform a transformation of the forward projection values in order to handle incorrect values in the transition region. We choose $(v_2 - v_1) \times u_t$ to be the size of the transition region, where $(v_2 - v_1)$ is the size of the ROI in v-direction and u_t corresponds to the number

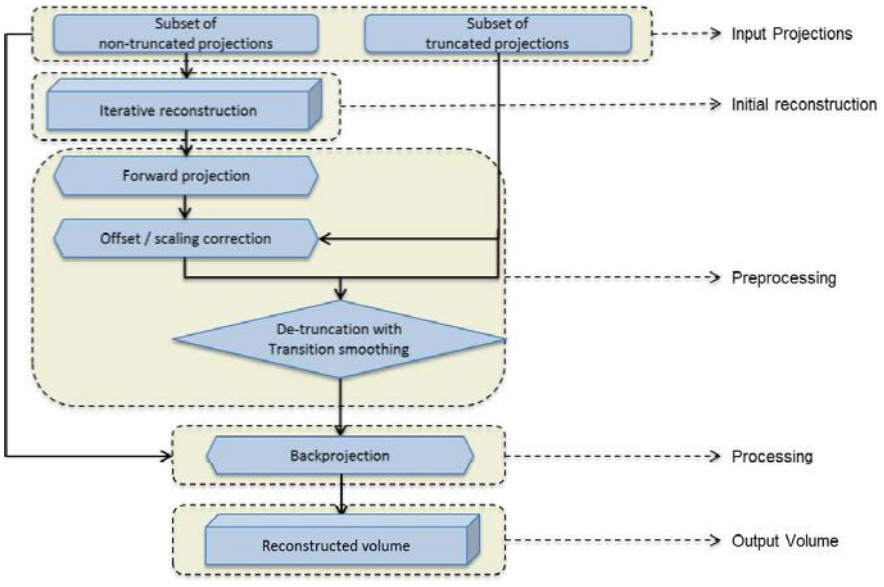

Fig. 2. Flowchart of the reconstruction approach.

of columns in the u-direction, e.g. $u_t = 60$. Similar to the suggested method described in [5], we designed two 2D parameter masks $A(\lambda_T, u, v)$ and $B(\lambda_T, u, v)$ (1) for each projection of the set of forward projections that correspond to the same angular position as a truncated projection. We used these filter masks to perform the scaling and offset correction of the forward projections

$$A = \frac{\sigma_{TR}}{\sigma_{FP}} \quad \text{and} \quad B = \mu_{TR} - A \cdot \mu_{FP} \tag{1}$$

where σ_{TR} and σ_{FP} correspond to the standard deviations, and μ_{TR} and μ_{FP} to the mean values of the transition region of the truncated projection $g_{TR}(\lambda, u, v)$ and the corresponding forward projection $g_{FP}(\lambda, u, v)$, respectively.

As a first step, the mean values and the standard deviations are calculated for each pixel (u, v) in the transition region over the entire column in u-direction and over the entire row in v-direction of the forward projection and the truncated projection. Filter values outside the transition region are obtained by constant extrapolation of the most outer filter values of the transition region in u-direction. Finally, the actual transformation of each pixel is achieved according to

$$g_{C,FP}(\lambda_T, u, v) = A(\lambda_T, u, v) \cdot g_{FP}(\lambda_T, u, v) + B(\lambda_T, u, v) \tag{2}$$

where $g_{C,FP}(\lambda_T, u, v)$ describes the corrected forward projection at rotation angle λ_T, which corresponds to the rotation angle of a truncated projection from the proposed acquisition scheme. The filter mask A is employed as the scaling correction parameter, while the filter mask B is used to compensate the offset problem.

Cosine filtering and combination By applying a cosine filtering step, we handle sudden changes of values at the boundary of the ROI and provide a smooth transition region in the combined projection data. Finally, the reconstruction is carried out by a standard FDK algorithm [2].

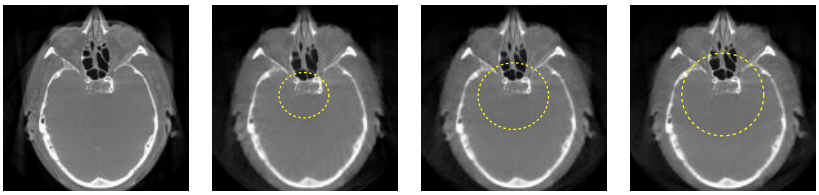

(a) FDK (b) ROI: 320x320 (c) ROI: 400x400 (d) ROI: 500x500

Fig. 3. Transversal slices of the reconstruction results. The grayscale window is [-1000 HU, 2500 HU]. Slice thickness is 0.4 mm and volume size is 512 × 512 × 350. The sparsity-level is $k = 10$. (a) Ground truth reconstruction (FDK on non-truncated data), (b) proposed reconstruction on partially truncated projection data from the proposed acquisition scheme at a small ROI size, (c) a medium ROI, (d) a large ROI.

3 Experiments

The developed algorithm is evaluated in a qualitative and quantitative manner using a clinical data set (data courtesy of St. Luke's Episcopal Hospital, Houston, TX, USA). It holds a full set of non-truncated projections. We used virtual truncation to simulate the collimator and to generate the truncated projections. The experiments were performed for different sparsity levels ($k \in \{1, 2, 4, 6, 8, 10\}$) as well as for three different collimation sizes (320×320 px, 400×400 px, 500×500 px). The VOI and the PR were evaluated separately and were visually compared to the ground truth (FDK on full set of non-truncated projection data). Standardized image quality metrics (correlation coefficient (CC), root mean square error (RMSE), both with respect to the FDK reconstruction on full set of non-truncated projection data) were used for a quantitative evaluation.

3.1 Results

Fig. 3 shows the reconstruction results for three different ROI sizes, which are visually compared to the ground truth. In Fig. 3(b), we observed slight streak artifacts at the bone structures of the head, which are decreasing with an increasing ROI size (Fig. 3(d)). Fig. 4 shows a rather comparable image quality in the PR for different levels of sparsity, indicating that the dose reduction associated with increasing sparsity levels comes with a much less pronounced degradation of image quality in the PR. Only a slight increase in streak artifacts can be observed in the PR at a higher sparsity level. In summary, both, for a decreasing ROI size (Fig. 3) as well as for an increasing sparsity level (Fig. 4), the degradation in image quality in the PR is rather low. In addition, details in the VOI are well preserved and no additional artifacts could be observed. Furthermore, a smooth transition region between the VOI and the PR is observed (Sec. 2.2).

In Fig. 5(a) and Fig. 5(b), quantitative results are shown for three different ROI sizes. For all ROI sizes, we notice that the RMSE of the PR is increasing rapidly with a higher sparsity, while the RMSE of the VOI increases substantially less. Furthermore, the CC of the PR decreases fast, while the CC decreases slow for the VOI even at an increasing sparsity level. The previous visual observation is also confirmed by the quantitative evaluation. Additionally, better results for both, the CC and RMSE are achieved within the VOI with increasing ROI size.

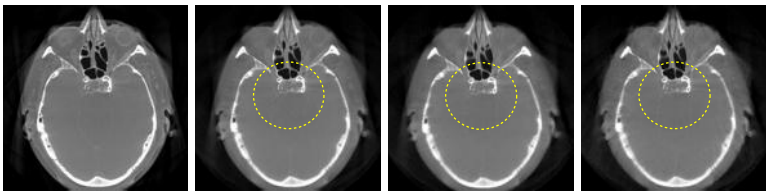

(a) FDK (b) k = 4 (c) k = 6 (d) k = 10

Fig. 4. Same slice and volume information as in Fig. 3. The ROI is 400× 400 px.(a) Ground truth, (b) proposed reconstruction at different sparsity levels.

Fig. 5. RMSE (a) and CC (b) of the PR and VOI from the reconstruction result at a medium ROI size of 400×400 px.

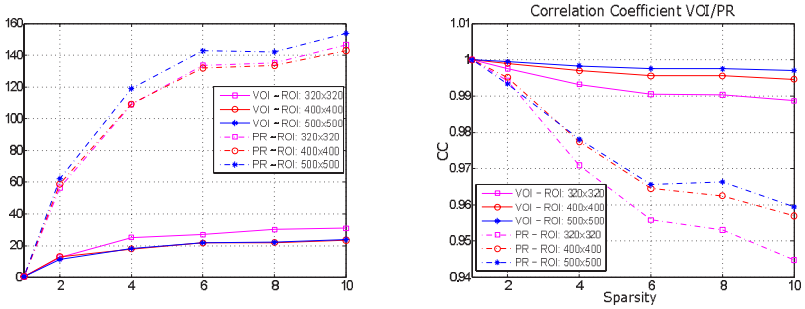

(a) RMSE, different ROI sizes

(b) CC, different ROI sizes

4 Discussion

We presented an algorithm that is tailored to dynamically collimated acquisitions and were able to obtain reconstruction results with a high image quality in the VOI, while promising results for the PR were achieved. By incorporating the sparse set of full FOV projections, we were able to not only improve the image quality of the VOI but also to obtain additional information in the PR region, while keeping the total radiation dose low. Furthermore, we showed that our algorithm is robust in terms of different ROI sizes as well as for an increasing level of sparsity.

Acknowledgement. The concepts and information presented in this paper are based on research and are not commercially available.

References

1. Leary D, Robar JL. CBCT with specification of imaging dose and CNR by anatomical volume of interest. Med Phys. 2014;41(1):011909.
2. Feldkamp L, Davis L, Kress J. Practical cone-beam algorithm. J Opt Soc Am A. 1984;1(6):612–9.
3. Robar JL, Parsons D, Berman A, et al. Volume-of-interest cone-beam CT using a 2.35 MV beam generated with a carbon target. Med Phys. 2012;39(7):4209–18.
4. Ritschl L, Bergner F, Fleischmann C, et al. Improved total variation-based CT image reconstruction applied to clinical data. Phys Med Biol. 2011;56(6):1545.
5. Kolditz D, Kyriakou Y, Kalender WA. Volume-of-interest (VOI) imaging in c-arm flat-detector CT for high image quality at reduced dose. Med Phys. 2010;37(6):2719–30.